

Article

Targeting Bioinformatics Predicted Biomarkers Associated with Cell Proliferation and Migration for Treating Gliomas: Preclinical Studies in a GL261 Mouse Model

Rheal A. Towner ^{1,2,3,*}, Nataliya Smith ², Debra Saunders ², Megan Lerner ⁴, Randy L. Jensen ⁵, James Battiste ³, Marya Ahmed ¹  and Jonathan D. Wren ⁶

¹ Department of Chemistry, University of Prince Edward Island, Charlottetown, PE C1A 4P3, Canada

² Advanced Magnetic Resonance Center, Oklahoma Medical Research Foundation, Oklahoma City, OK 73104, USA

³ Department of Neurosurgery, Stephenson Cancer Center, University of Oklahoma Health Sciences Center, Oklahoma City, OK 73104, USA

⁴ Department of Surgery Research Laboratory, University of Oklahoma Health Sciences Center, Oklahoma City, OK 73104, USA

⁵ Huntsman Cancer Institute, University of Utah, Salt Lake City, UT 84112, USA

⁶ Genes & Human Disease Research Program, Oklahoma Medical Research Foundation, Oklahoma City, OK 73104, USA

* Correspondence: rheal.towner@upei.ca

Abstract: We previously reported on the experimental validation of several in silico-predicted glioma biomarkers (e.g., Plexin-B2 (PLXNB2), SLIT3, and Spondin-1 (SPON1)) that were found to be higher in human high-grade gliomas (HGGs). In this study, we validated their therapeutic potential by investigating antibody therapies against these three biomarkers in a preclinical mouse GL261 high-grade glioma model. Efficacies for antibody therapies against these biomarkers were assessed by survival and tumor volumes, biomarker expressions, cell invasion and proliferation, and bioinformatics gene/protein associations. Antibodies against PLXNB2, SLIT3, or SPON1 were effective in significantly reducing tumor volumes and increasing animal survival. With immunohistochemistry (IHC), these biomarkers were highly expressed in human HGGs, as well as in mice tumors. From IHC, CD44v6 was significantly decreased for all three antibody treatments, compared to UT GL261 tumors. Bioinformatics suggested that targeting either PLXNB2 or SPON1 may have a major effect on HGG cell migration and invasion (validated with CD44v6 IHC), whereas targeting SLIT3, in addition to affecting cell invasion, may also affect cell proliferation (not validated with Ki67 IHC). These results indicate that targeting these three biomarkers could add to the therapeutic arsenal against high-grade gliomas and that antibodies against them could be considered for clinical translation.

Keywords: high-grade glioma (HGG); GL261; antibody therapies; Plexin-B2; SLIT-3; Spondin-1; molecular-targeted MRI (mt-MRI); bioinformatics; Ki67; CD44



Citation: Towner, R.A.; Smith, N.; Saunders, D.; Lerner, M.; Jensen, R.L.; Battiste, J.; Ahmed, M.; Wren, J.D. Targeting Bioinformatics Predicted Biomarkers Associated with Cell Proliferation and Migration for Treating Gliomas: Preclinical Studies in a GL261 Mouse Model. *Neuroglia* **2023**, *4*, 69–86. <https://doi.org/10.3390/neuroglia4010006>

Academic Editor: Stefania Ceruti

Received: 12 January 2023

Revised: 2 March 2023

Accepted: 7 March 2023

Published: 15 March 2023



Copyright: © 2023 by the authors. Licensee MDPI, Basel, Switzerland. This article is an open access article distributed under the terms and conditions of the Creative Commons Attribution (CC BY) license (<https://creativecommons.org/licenses/by/4.0/>).

1. Introduction

The most recent CNS5 (Central Nervous System) World Health Organization (WHO) classifications for adult-type diffuse gliomas, which divides these tumors by IDH (isocitrate dehydrogenase 1) mutation, 1p/19q-codeletion, and histological grade, are astrocytoma, IDH mutant (Grade 2 to 4); oligodendroglioma, IDH mutant and 1p/19q-codeleted (Grades 2 and 3); and glioblastoma, IDH-wildtype (Grade 4) [1,2]. NCCN (National Comprehensive Cancer Network) guidelines currently separate treatment recommendations according to tumor grade and subtype. For instance, the standard of care (SOC) for Grade 2 oligodendroglioma, with a favorable risk profile (gross total resection and ages less than 40 years old), is observation and treatment at recurrence, but the SOC for glioblastoma

(Grade 4) is maximal feasible resection followed by radiotherapy and concurrent and adjuvant temozolomide chemotherapy, with an overall survival of only 14.6 months [3]. The concern for all of these glioma subtypes is the chance and speed of recurrence despite the SOC. It is important to consider that there are genetic, epigenetic, and environmental heterogeneities that exist within each individual glioma and that intra-tumoral heterogeneities result in several phenotypic cellular heterogeneities, which lead to multiple mechanisms of therapeutic resistance that result in highly adaptable and resistant tumors [4].

Treatments for primary brain tumors are complicated by the different tumor traits of primary or secondary gliomas (low-grade lesions transformed into high-grade tumors), as well as the difficulties associated with identifying radiation necrosis, tumor progression, and pseudoprogression with standard magnetic resonance imaging (MRI) [5]. More precise diagnosis, prediction of prognosis, and assessing tumor response to current and recent therapies may offer more promise with radiomics and radio-genomics derived from morphological, textural, and functional characteristics obtained from quantitative voxel-level MR image metrics [5]. Novel emerging radiomic techniques using machine learning and fractal-based analyses have the potential capabilities for improving both diagnostic and prognostic accuracies for gliomas [6]. Over the past decade or so, molecular diagnostic capabilities involving the use of chemical-, peptide-, antibody-, and nanoparticle-based imaging probes have also been developed to target specific molecules in gliomas, which can be visualized with different multimodality clinically relevant molecular imaging approaches, such as positron emission tomography (PET), single-photon emission computed tomography (SPECT), near-infrared fluorescence (NIRF), and/or magnetic resonance imaging (MRI) [7].

New feasible or potential targets for the treatment of gliomas, especially IDH-wild-type glioblastoma, are now being considered [3]. Classical biomarker targets, such as p53, the retinoblastoma (RB) pathway, and an epidermal growth factor receptor (EGFR) gene alteration, have unfortunately failed due to complex regulatory networks [3]. More recently, there is an interest in immunotherapies (e.g., immune checkpoint molecules, tumor-associated macrophages, dendritic cell vaccines, CAR-T (chimeric antigen receptor T)) and targeting the tumor microenvironment [3]. The appeal of selecting biomarkers for more personalized targeted therapies is becoming extremely attractive. Our focus for the past decade has been to try and identify new therapeutic targets for high-grade gliomas that can potentially be translated clinically, as well as develop molecular imaging approaches to visualize these new targets *in vivo* using preclinical models.

We previously reported on the experimental validation of a few *in silico*-predicted glioma biomarkers that were found to be significantly higher in human high-grade gliomas (hHGGs) than low-grade gliomas [8]. These included SLIT3, Plexin-B2 (PLXNB2), and Spondin-1 (SPON1). Plexins are a family of genes that are expressed in several organ systems and have been implicated in cell movement and cell–cell interaction [9]. PLXNB2 has been previously reported to be related to the negative regulation of interleukin-12/interleukin-23p40 in dendritic cells [9]. Plexins have been identified as cell surface receptors widely studied in the nervous system, where they mediate migration and morphogenesis through the Rho family of small GTPases [10]. PLXNB2 has been found to be exceedingly expressed in cells of the innate immune system in the mouse, including macrophages and dendritic cells, and may serve as a negative regulator of basal cell motility [9]. PLXNB2 is related to genes that control extracellular matrix remodeling (MMP1, TGF β 1, COL2A1, COL1A1/2) and angiogenesis (VEGF- α and the integrin-binding protein IGFBP3) [2]. The SLIT3 gene at human chromosome 5q34-q35.1 is involved in encoding large secreted proteins functioning as ligands for Roundabout (ROBO) receptors, and the SLIT-ROBO signaling pathway is implicated in angiogenesis and endothelial cell migration [11]. SPON1 encodes a secreted extracellular matrix (ECM) glycoprotein (F-spondin/VSGP) [12]. SPON1 is connected to genes related to cell invasion or migration, such as MMPs, TGF β 1 (transforming growth factor β 1), several collagen genes, and CD44; endothelial cells (integrin ITGB1/3); and the epidermal growth factor receptor [13–15].

According to The Human Protein Atlas, which uses the TCGA database for human gliomas of various grades, PLXNB2 has high expression in 120 out of 153 glioma patients (78.4%), whereas SLIT3 and SPON1 had high expression in 47 and 76, respectively, out of 153 patients (30.7 and 49.7%, respectively). It is interesting that all three biomarkers are listed in The Human Protein Atlas as being not prognostic for gliomas. However, previously, we reported that all three of these biomarkers are diagnostic for human high-grade gliomas (hHGGs) in an independent study [8]. If the TCGA data is made up of both low- (TCGA-LGG: 515 samples; 46%) and high-grade (TCGA-GBM: 599 samples; 54%) gliomas, then this could explain the discrepancy (<https://portal.gdc.cancer.gov> (accessed on 4 November 2022)), as our data found high expressions of PLXNB2, SLIT3, and SPON1 only in hHGGs but not in hLGGs, i.e., the hLGG data in the TCGA database may be diluting the overall expression for all gliomas as reported in The Human Protein Atlas. Larger independent studies would need to be conducted on both hHGGs and hLGGs for the three biomarkers in question.

In this study, we validated the therapeutic potential of PLXNB2, SLIT3, and SPON1 by investigating antibody therapies against each of these three biomarkers in a preclinical mouse GL261 high-grade glioma (HGG) model in syngeneic C57BL6/J mice. We also established that these three biomarkers are highly expressed in both a mouse GL261 HGG model, using in vivo molecular-targeted MRI (mt-MRI), as well as translationally in human HGGs, from immunohistochemistry (IHC). Bioinformatics was also used to link other genes and proteins highly associated with these biomarkers, which provides some insight regarding their broad activities against HGG tumorigenesis. Bioinformatics predicted that all three of these biomarkers were associated with cell proliferation and cell migration, and so we used IHC in the GL261 mouse model to look at the expressions of Ki67 and CD44v6, respectively.

2. Materials and Methods

2.1. Glioma Model

Two-month-old male C57BL6/J mice (Harlan Laboratories, Indianapolis, IN, USA) were intracerebrally implanted with mouse GL261 (104) glioma cells (National Cancer Institute, Frederick, MD, USA) as previously performed [16]. All animal studies were approved by the Oklahoma Medical Research Foundation Institutional Animal Care and Use Committee in accordance with the Guide for the Care and Use of Laboratory Animals as adopted and promulgated by the U.S. National Institutes of Health.

2.2. Treatments

GL261 tumor-bearing mice were treated with either anti-PLXNB2 ($n = 5$) (I-16 (#sc-34504, Santa Cruz Tech, Santa Cruz, CA, USA), 2 mg/kg in 100 μ L saline every 3 days for up to tumor maximum); anti-SLIT3 ($n = 7$) (H-54 (#sc-28946, Santa Cruz Biotech, Santa Cruz, CA, USA), 1.5–2.0 mg/kg in 100 μ L saline every 3 days for up to tumor maximum); or anti-SPON1 ($n = 7$) antibodies (N-19 (#sc-49006, Santa Cruz Tech, Santa Cruz, CA, USA), 1 mg/kg in 100 μ L saline every 3 days for up to tumor maximum). Antibodies (Santa Cruz) used described in the Methods were available when we conducted the antibody treatments in the GL261 mouse HGG model; however, these have been recently discontinued by the manufacturer. We have searched and found comparable antibodies for the extracellular regions for either PLXNB2, SLIT3, or SPON1. These include an alternative for anti-PLXNB2 antibody (AF683b, R&D Systems, Minneapolis, MN, USA), an alternative for anti-SLIT3 antibody (DF9909, Affinity Biosciences, Cincinnati, OH, USA), and an alternative for anti-SPON1 antibody (DPABH-08849, Creative Diagnostics, Shirley, NY, USA). Untreated mice ($n = 12$) served as controls for statistical comparison. Previous studies conducted by our group found no statistical differences between untreated and isotype antibody (non-specific IgG) treatment [17]. Treatments were initiated when the tumors reached 10–20 mm³ in volume, as determined by morphological MRI. As the tumor take rate was approximately 90%, we ensured there were sufficient mice to have a minimum of 5–7 mice per treatment

group. We incorporated more untreated mice in order to ensure that there were sufficient control mice to compare with treatment cohorts during MRI investigations, resulting in a larger no. for this group. All antibody treatments were administered via a tail vein catheter. Doses for antibody treatments were selected based on similar previous studies [17]. Animal percent survivals were obtained, with the proviso that all mice were euthanized when tumor volumes reached $\geq 150 \text{ mm}^3$. In some instances, mice died overnight before we could obtain viable tissues for histological investigations, but survival data were still obtained.

2.3. MRI Molecular-Targeting Agent Synthesis

Antibody-conjugated MRI contrast agents were prepared according to the previously reported methods [17], using the antibodies described above. Biotinylated albumin conjugates were prepared using a sulfo-NHS crosslinker. Biotinylated BSA-albumin was dialyzed and reacted with diethylene triamine penta acetic acid anhydride (DTPA) to develop a gadolinium-chelating construct. Gd(III) chloride was then gradually added and the mixture was reacted at 4°C for 24 h to yield Gd-DTPA-albumin. Gd-based molecular probes were then prepared by reacting Gd-DTPA-BSA with antibodies (either anti-PLXNB2, anti-SLIT3, or anti-SPON1) in the presence of a sulfo-NHS crosslinker.

2.4. MRI

MRI experiments were carried out on a Bruker BioSpec 7.0 Tesla/30-cm horizontal-bore magnet imaging system. Animals were immobilized by using 1.5–2.5% isoflurane and 0.8 L/min O_2 and placed in a 72-mm quadrature volume coil for signal transmission, and a surface mouse-head coil was used for signal reception. T2-weighted imaging was acquired as previously performed by our group [17]. Morphological images were obtained from days 10–11 following the intracerebral implantation of GL261 cells and every 7–10 days until tumors reached $\geq 150 \text{ mm}^3$ in volume (maximum tumor volumes).

Molecular MRI

Molecular MRI was executed when the tumor volumes were close to their maximum tumor volumes ($120\text{--}180 \text{ mm}^3$). A variable-TR RARE sequence (rapid acquisition with refocused echoes, with multiple TRs of 200, 400, 800, 1200, and 1600 ms, TE of 15 ms, FOV of $3.5 \times 3.5 \text{ cm}^2$, matrix size of 256×256 , and a spatial resolution of 0.137 mm) was used to obtain T1-weighted images before and after the administration of probe or control contrast agents. Relative probe (contrast agent) expressions were calculated to assess the levels of PLXNB2, SLIT3, and SPON1 probes in each animal. A contrast difference image was created from the pre- and (90 min) post-contrast datasets for the slice of interest, by computing the difference in signal intensity between the post-contrast and the pre-contrast image on a pixel basis, as described previously [17]. From a difference (post-contrast minus pre-contrast) image, ten regions of interest (ROI) of equal size (0.05 cm^2) were drawn within areas with the highest MRI signal intensities in the tumor parenchyma and contralateral side of the brain for each animal after either the PLXNB2, SLIT3, or SPON1 probes were injected at the TR 800 ms. The values obtained from the ROIs in the tumor regions were normalized to the corresponding contralateral sides. An overlay of the contrast difference image and T1-weighted image was generated using the 3D Analysis Software for Life Sciences Amira[®] (Fei, Hillsboro, OR, USA) [17].

2.5. Histology and Immunohistochemistry

2.5.1. Human Tissue Samples

The human tissue sample portion of the study was conducted in compliance with the University of Utah Health Sciences Center Institutional Review Board in accordance with the Declaration of Helsinki. For IHC analysis, tissue from 50 patients with high-grade gliomas (21 female, 29 male), including 40 GBM, 6 anaplastic astrocytomas, and 4 anaplastic oligodendrogliomas, was compared with tissue from 21 patients (10 female, 11 male) with tumors classified as low-grade gliomas (11 benign oligodendrogliomas, 10 low-grade

astrocytomas). Antibodies (Abs) to Plexin-B2, Slit homolog (SLIT3), and spondin1 were available commercially (Plexin-B2 Ab (I-16), SLIT3 Ab (F-15), and F-spondin Ab (S-17) were all obtained from Santa Cruz Biotechnology). The procedures followed were completed as previously reported [8,18]. A score of 0–4 was assigned based on the percentage of cells stained in a given field: 0 = 0–25%, 1 = 25–50%, 2 = 50–75%, 3 = 75–100%, and 4 = 100%. Positive expression was determined for scores of 2–4, whereas negative expression was established for scores of 0 and 1. Percent survivals for the GBM, anaplastic astrocytoma, and anaplastic oligodendroglioma patients were 0.0%, 0.0%, and 50.0%, respectively. Percent survival values for benign oligodendroglioma and low-grade astrocytoma patients were 27.3% and 70.0%, respectively.

Toluidine blue (0.1%) counterstain was used (15 s). IHC was performed using the Vectastain ABC Kit (Vector Laboratories). Negative controls were performed by replacing the primary Ab with nonimmune serum. Slides were examined using an Olympus BX41 microscope. Under 200× magnification (10 ocular × 20 objective), slides were scored by 2 investigators blinded to the specimen tumor grade or patient information. In prior papers, we have demonstrated that this method is very reproducible, with good interrater reliability ($p = 0.99$, 95% confidence interval (CI) = 0.99–1.00) and intrarater reliability ($p = 0.96$, 95% CI = 0.92–0.99). Each investigator independently reviewed the slide at low power and at random high-power fields when determining the IHC score.

We acknowledge the evolving complexities of using molecular classifications; however, there is still some validity in using high- and low-grade dichotomization. For instance, all of the HGG tumors in this study were IDH1^{WT}, and all of the low-grade tumors used in this study were IDH1 mutated. For a preliminary study where the numbers are relatively low, we decided to combine our tumors into HGG and LGG categories.

2.5.2. Mouse Tissue Samples

All mice were sacrificed after the last MRI scan. The brain of each animal ($n = 4$ /group) was removed, preserved in 10% neutral buffered formalin, and processed routinely, as described previously [17].

Five-micron-thick histological sections, embedded in paraffin and mounted on HistoBond® Plus slides (Statlab Medical Products, Lewisville, TX, USA) were rehydrated and washed in Tris Buffered Saline. Antigen retrieval (pH 6 Citrate Antigen Unmasking Solution; cat# H-3300; Vector Labs Inc., Burlingame, CA, USA) was accomplished via twenty minutes in a steamer followed by thirty minutes of cooling at room temperature. Sections were treated with a peroxidase-blocking reagent (Bloxall, cat# SP-6000; Vector Laboratories, Inc., Burlingame, CA, USA) to inhibit endogenous peroxidase activity. Slides for SA-HRP immunohistochemistry for the molecular-targeted MRI study were incubated with R.T.U. streptavidin (SA) and peroxidase (HRP) (cat # SA-5704; Vector Lab, Burlingame, CA, USA) in a humidified chamber for 30 min at room temperature. Appropriate washes were in TBS. The SA-HRP targets the biotin moieties of the antibody probes (either anti-PLXNB2, anti-SLIT3, or anti-SPON1 molecular-targeted gadolinium-based MRI probes). Slides were incubated with NovaRed® (cat# SK-4805; Vector Laboratories, Inc., Burlingame, CA, USA) chromogen for visualization. Counterstaining was carried out with Hematoxylin QS Nuclear Counterstain (Vector laboratories, Burlingame, CA, USA). This is similar to what was previously published [17]. Appropriate positive and negative tissue controls were used. Isotype controls were used for negative antibody staining, and positive/negative tissue staining was based on previous stains on other tissues used in the lab (as prescribed by the vendors). For IHC staining, rabbit antibodies were used for Ki-67 (cat# NB600-1209, 2 µg/mL, Novus Biologicals, Littleton, CO, USA) and CD44v6 (cat# orb13319, 1.7 µg/mL, Biorbyt Ltd., San Francisco, CA, USA) immunohistochemistry (IHC). Both antibodies were diluted 1:300. The sections were processed using the ImmPRESS™ VR Reagent Anti-Rabbit IgG Peroxidase (VLI cat #MP-6401) [17]. Antigen retrieval (pH6 citrate antigen unmasking solution; VLI cat#H-3300) was accomplished for 20 min in a steamer followed by 30 min of cooling at room temperature. Sections were treated with a peroxidase-blocking reagent

(Bloxall, VLI cat#SP-6000) followed by 2.5% normal horse serum to inhibit non-specific binding [17]. Antibodies were applied to each section and, following incubation overnight at 4 °C in a humidified chamber, sections were washed in TBS and reagents were applied according to the manufacturer's directions. Slides were incubated with NovaRed[®] as described above. Counterstaining was carried out as described above (similar to what was previously published [17]). Appropriate positive and negative tissue controls were used. Isotype controls for negative antibody staining and positive/negative tissue staining were as described above.

To characterize IHC positivity levels, five regions of interest (ROIs), secured digitally (20×) using a Leica-Aperio CS whole-slide scanner, were identified in each case. Only areas containing tumor tissue were analyzed, excluding areas with necrosis and/or significant artifacts. The number of positive pixels was divided by the total number of pixels (negative and positive) in the examined area. ROIs were analyzed using Leica-Aperio ImageScope and Leica-Aperio Tool Box (pixel count algorithm) (Leica Biosystems, Buffalo Grove, IL, USA).

2.6. GAMMA and STRING

GAMMA (GlobAl Microarray Meta-Analysis) is a method used to compile and analyze transcriptional correlation networks using publicly available microarray data [19]. Briefly, it operates on a “guilt-by-association” principle, whereby the 40 most highly correlated transcripts across experimental conditions are analyzed for their commonalities using either Gene Ontology (GO) or the text-mining of PubMed abstracts. Statistically significant annotations tend to overlap heavily with known annotations for genes with established functions. Its strength lies in inferring function for unknown or poorly known transcripts. Several prior studies have shown that predicted phenotypes for unknown/poorly-known transcripts were observed experimentally using gene perturbation experiments [8,20–22]. As GAMMA uses literature mining to identify associations between genes and diseases such as gliomas (and synonymous terms), if there are updated classifications, the GAMMA-associated predictions would only be impacted if the data contained new terms. It is important to note that predicted associations rely upon the prior literature, which will not be updated when new terminology or classifications are included. The PubMed literature network used to generate these predictions was constructed using all abstracts available on 1 November 2022.

The STRING database [23] integrates both known and predicted physical and functional associations between proteins, from several sources: (1) text-mining the literature, (2) databases of interaction experiments, (3) predicted interactions from co-expression and genomic context, and (4) ortholog interactions. The web interface to STRING version 11 was used to generate the PPI networks with default parameters.

2.7. Statistical Analysis

Statistical analyses were conducted using GraphPad Prism 9 (GraphPad Prism 9.3.1 Software, San Diego, CA, USA). Tumor volumes, positivity for CD44v6 and Ki67, and the PLXNB2, SLIT3, or SPON1 levels from molecular targeting were reported as means ± standard deviation. Kaplan–Meier survival curves and a Log-rank (Mantel–Cox) test were used to compare the survival times among the untreated and treated groups. ANOVA testing (one-way, multiple comparisons) was used when comparing multiple treatment groups for tumor volumes and to assess the differences between the means of untreated and anti-PLXNB2-, anti-SLIT3-, or anti-SPON1-treated GL261 glioma mice for CD44v6 or Ki67 IHC positivity levels in tumor and contralateral regions. Tukey's multiple comparison tests were used for multiple comparisons. Student *t*-tests (independent samples, two-tailed *t*-tests) were used when comparing the mt-MRI IgG, PLXNB2-, SLIT3-, or SPON1-probe levels. All *p* values < 0.05 were considered statistically significant. The sample size was set based on the expected level of variability (standard deviation/mean) based on what has been observed in previous, similar studies. More mice (*n* = 12) were assigned to the

control, as this is the reference level for most comparisons. A power analysis with the R function “power.t.test” shows that $n = 5$ to 7 mice per treatment group ensures reaching common statistical parameters of about 0.8 power (0.75 for $n = 5$, 0.85 for $n = 7$) and 0.05 type 1 error rate on a standard two-sided t -test assuming the difference between group means will exceed 1.5, given the expected group standard deviation.

3. Results

3.1. Human Protein Expressions for PLXNB2, SLIT3, or SPON1: Immunohistochemistry (IHC)

Human HGGs demonstrate high levels of expression of all three biomarkers, PLXNB2, SLIT3, and SPON1, as shown in Figure 1, where the percentage of patient expression for each biomarker in HG (high-grade) is 80% or higher.

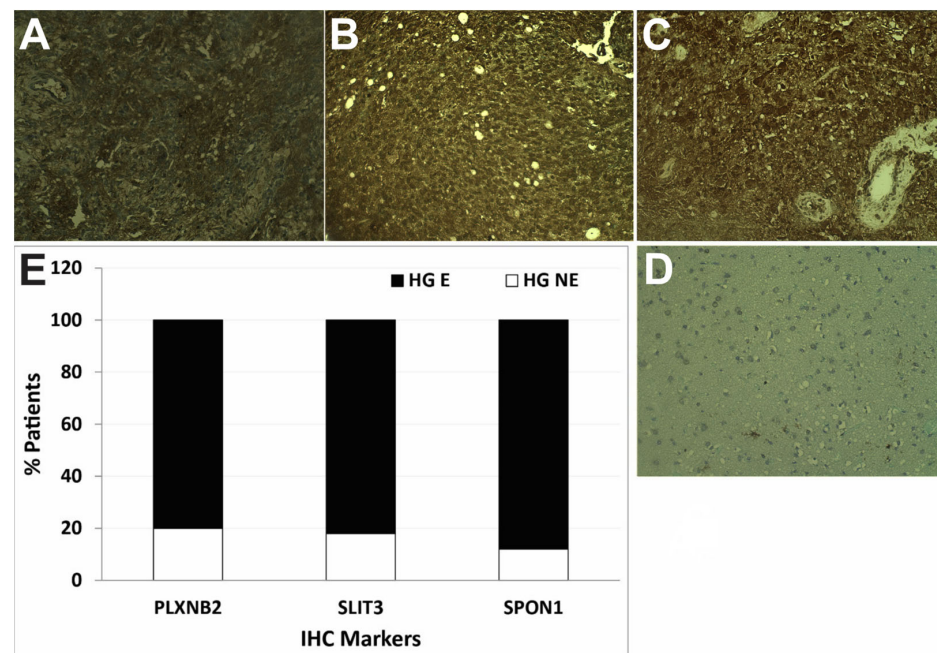


Figure 1. Expressions of PLXNB2, SLIT3, and SPON1 in human high-grade gliomas. Representative immunohistochemistry (IHC) images for PLXNB2 (A), SLIT3 (B), and SPON1 (C) in human GBM tumor sections. (D) Negative control in a low-grade glioma for SLIT3. Magnification is 20 \times for slides in (A–D). (E) Percentage (%) of patient protein expression (IHC) for PLXNB2, SLIT3, and SPON1 in high-grade (HG) gliomas highly expressed (HG E) or not expressed (HG NE). The % of patient expression for each biomarker in HG was 80% or higher.

3.2. Mouse Tumor Responses to Antibody Therapies against PLXNB2, SLIT3, or SPON1

Antibody treatment against PLXNB2 was found to significantly increase mouse survival in GL261 tumor-bearing mice when compared to untreated (UT) controls ($p < 0.01$) (Figure 2A). Tumor volumes for PLXNB2 antibody-targeted treated mice were also significantly less than UT controls ($p < 0.01$) (Figure 2B). Representative tumor volume morphological images for UT controls, compared to anti-PLXNB2-treated GL261 tumor-bearing mice, are shown in Figure 2C,D, respectively. Antibody treatment against SLIT3 was also found to significantly increase mouse survival in GL261 tumor-bearing mice when compared to UT controls ($p < 0.0001$) (Figure 2E). Tumor volumes for SLIT3 antibody-targeted treated mice were also significantly less than UT controls ($p < 0.0001$) (Figure 2F). Representative tumor volume morphological images for UT tumors, compared to anti-SLIT3-treated GL261 tumor-bearing mice, are shown in Figure 2G,H, respectively. Antibody treatment against SPON1 was also found to significantly increase mouse survival in GL261 tumor-bearing mice when compared to UT controls ($p < 0.05$) (Figure 2I). Tumor volumes for SPON1 antibody-targeted treated mice were also significantly less than UT controls ($p < 0.001$) (Figure 2J). Representative tumor volume morphological images for UT, compared to

anti-SPON1-treated GL261 tumor-bearing mice, are shown in Figure 2K,L, respectively. A treatment schematic and summarized outcomes are shown in Figure 2M.

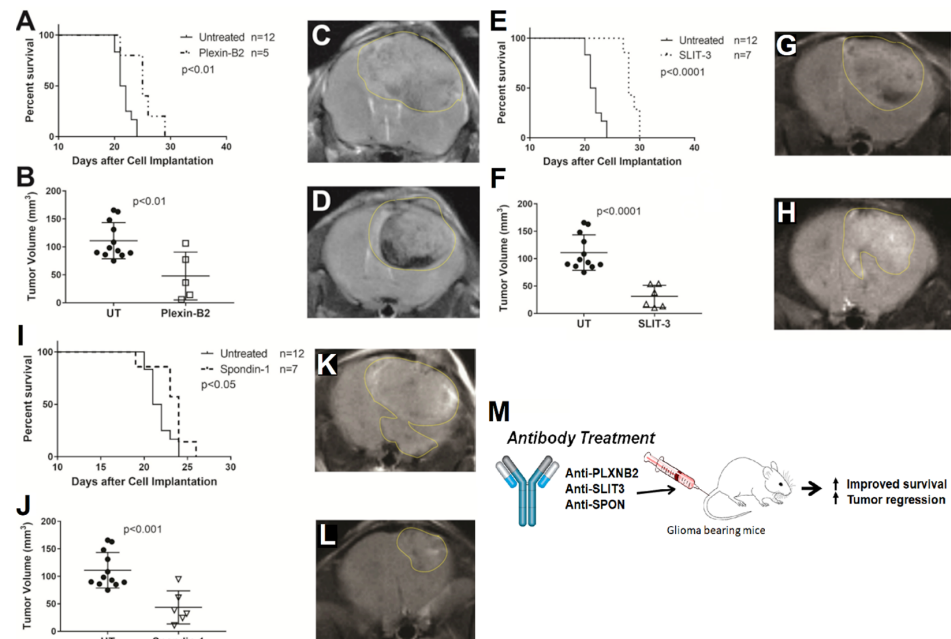


Figure 2. Antibodies against PLXNB2, SLIT3, or SPON1 are effective against GL261 orthotopic tumors. Common untreated data sets were used to compare each antibody treatment separately. (A) Survival curve for untreated and PLXNB2-antibody-treated GL261 tumor-bearing mice. There was a significant increase in the percentage of survival for PLXNB2-antibody-treated GL261 tumor-bearing mice ($n = 5$) compared to untreated controls ($n = 12$) ($p < 0.01$; $p = 0.006$). (B) Tumor volumes (mm^3), as measured from morphological MRI for untreated and PLXNB2-antibody-treated GL261 tumor-bearing mice at 21 days (treatment groups) from GL261 tumor cell implantations or maximum tumor volumes for UT tumors (average survival of 21 days). There was a significant decrease in tumor volumes for PLXNB2-antibody-treated GL261 tumor-bearing mice ($n = 5$) compared to untreated controls ($n = 12$) ($p < 0.01$; $p = 0.003$). Representative morphological MR images in untreated (C) and PLXNB2-antibody-treated (D) GL261 tumor-bearing mice. (E) Survival curve for untreated and SLIT3-antibody-treated GL261 tumor-bearing mice. There was a significant increase in the percentage of survival for SLIT3-antibody-treated GL261 tumor-bearing mice ($n = 7$) compared to untreated controls ($n = 12$) ($p < 0.0001$). (F) Tumor volumes (mm^3), as measured from morphological MRI for untreated and SLIT3-antibody-treated GL261 tumor-bearing mice. There was a significant decrease in tumor volumes for SLIT3-antibody-treated GL261 tumor-bearing mice ($n = 6$) compared to untreated controls ($n = 12$) ($p < 0.0001$). Representative morphological MR images in untreated (G) and SLIT3-antibody-treated (H) GL261 tumor-bearing mice. (I) Survival curve for untreated and SPON1-antibody-treated GL261 tumor-bearing mice ($n = 7$) compared to untreated controls ($n = 12$) ($p < 0.05$; $p = 0.03$). It should be noted that with Bonferroni correction (all treatment groups compared), the p -value comparing UT to SPON1 for survival drops to $p = 0.09$. (J) Tumor volumes (mm^3), as measured from morphological MRI for untreated and SPON1-antibody-treated GL261 tumor-bearing mice. There was a significant decrease in tumor volumes for SPON1-antibody-treated GL261 tumor-bearing mice ($n = 6$), compared to untreated controls ($n = 12$) ($p < 0.001$). Representative morphological MR images in untreated (K) and SPON1-antibody-treated (L) GL261 tumor-bearing mice. Tumor boundaries are traced with a faint yellow line. (M) Antibody treatment schematic and summarized results. Kaplan–Meier survival curves and a Log-rank (Mantel–Cox) test were used to compare the survival times among the untreated and treated groups. ANOVA testing (one-way, multiple comparisons—Tukey’s multiple comparisons test) was used when comparing multiple treatment groups for tumor volumes.

3.3. Mouse GL261 Protein Expressions for PLXNB2, SLIT3, or SPON1: Molecular-Targeted MRI

In vivo protein expressions for the three biomarkers, PLXNB2, SLIT3, and SPON1, are shown in Figure 3 with the use of mt-MR imaging probes for each (anti-PLXNB2-, anti-SLIT3-, or anti-SPON1-antibodies conjugated to albumin-Gd-TPA-biotin constructs). Confirmation of the binding affinities of each probe was determined by targeting streptavidin-horse radish peroxidase (SA-HRP) to the biotin moieties of each probe, compared to non-specific IgG probe treatment. The synthesis of the MRI molecular-targeting probes and a summary of the findings are depicted in Figure 3K.

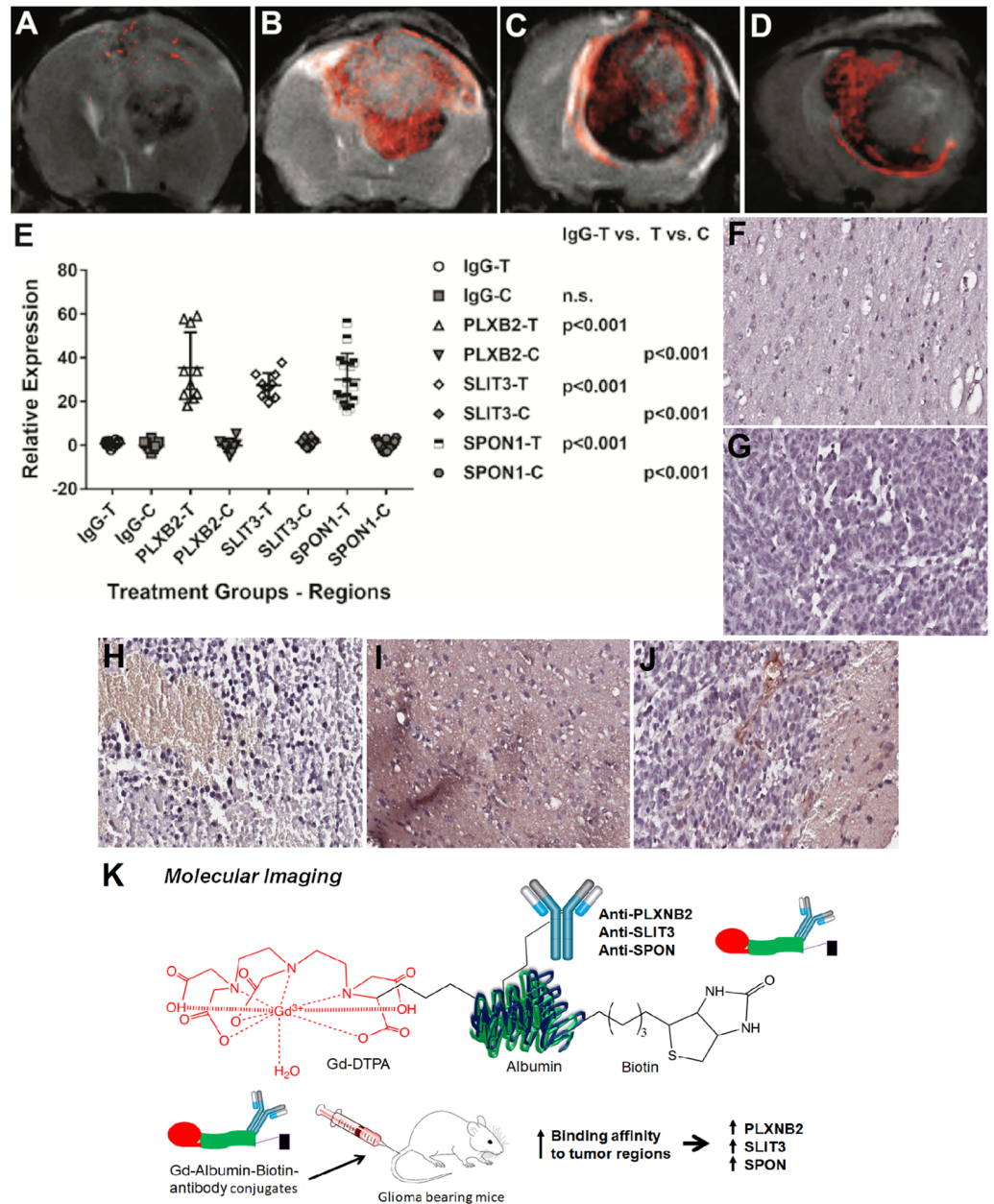


Figure 3. PLXNB2, SLIT3, and SPON1 are all highly expressed in untreated GL261 tumor-bearing mice, as determined from in vivo mt-MRI using specific probes for each biomarker. Images were obtained at maximum tumor volumes (approx. 21 days from GL261 cell implantations). Representative mt-MRI contrast difference images (false-colored in red) overlaid on top of morphological MR images (grayscale) for non-specific IgG (A), PLXNB2 (B), SLIT3 (C), and SPON1 (D). Probe construct bases were a Gd-DTPA-albumin-biotin combination, where the specific antibody (anti-PLXNB2, anti-SLIT3, or anti-SPON1) was conjugated directly to the albumin linker. (E) Relative expression of non-specific

Gd-DTPA-albumin-IgG-biotin, Gd-DTPA-albumin-anti-PLXNB2-biotin, Gd-DTPA-albumin-anti-SLIT3-biotin, Gd-DTPA-albumin-anti-SPON1-biotin probes in tumor (T) or contralateral (C) brain regions. $n = 5$ /group with 5-6 ROIs per animal in each region. There was a significant increase in each biomarker's relative expression in the tumor regions when compared to the non-specific IgG tumor regions ($p < 0.001$ for each). Each biomarker's relative expressions were also significantly increased when comparing tumor vs. contralateral regions ($p < 0.001$ for each). Representative tissue sections of streptavidin-horse radish peroxidase (SA-HRP) targeting biotin moieties of anti-PLXNB2 (H), anti-SLIT3 (I), or anti-SPON1 (J) probes, indicating selective binding in tumor regions. Control SA-HRP in normal brain (F) or tumor region (G) of a GL261-tumor bearing mouse treated with non-specific IgG. All histology slides are $20\times$ magnifications. (K) mt-MRI probe synthesis and treatment schematic and summarized results. Student *t*-tests (independent-samples, two-tailed *t*-test) were used to assess the differences between means of the mt-MRI IgG, PLXNB2-, SLIT3-, or SPON1-probe levels.

3.4. Mouse GL261 Protein Expressions for CD44v6 or Ki67 following Antibody Treatments

IHC staining for CD44v6 and Ki67 is shown in Figure 4. CD44v6 was found to be significantly less in the antibody therapies targeting PLXNB2, SLIT3, or SPON1, compared to untreated (UT) tumors (Figure 4A–F). Ki67 was found to be significantly less in the antibody therapies targeting PLXNB2 or SPON1 compared to untreated (UT) tumors, but not for SLIT3 (Figure 4G–L). The treatment schematic and summarized findings are shown in Figure 4M.

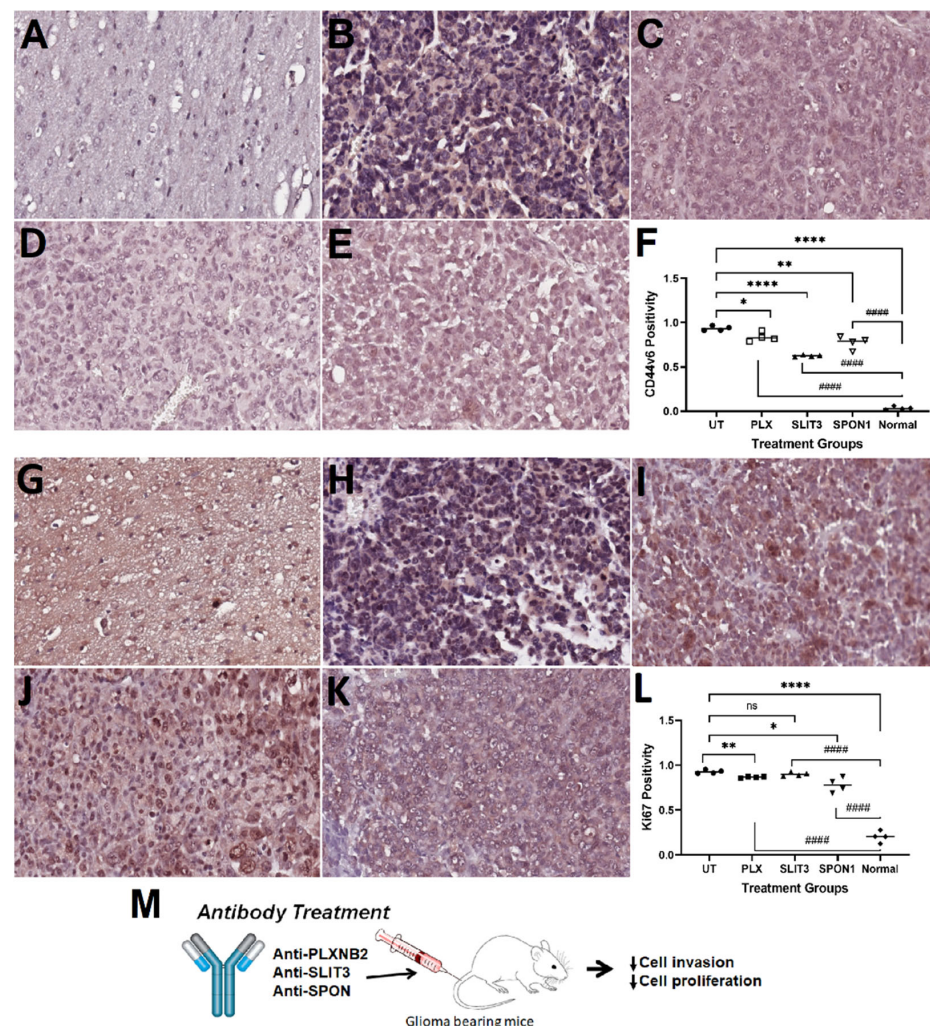


Figure 4. Immunohistochemistry (IHC) staining for CD44v6 in normal (A), untreated (UT) (B), and antibody treatments targeting plexin-B2 (PLX) (C), SLIT-3 (SLIT3) (D), and SPON-1 (SPON1) (E).

(F) Positivity values for CD44v6 levels in tumor regions from UT (closed circles), PLX (open squares), SLIT3 (closed triangles), and SPON1 (open inverted triangles) antibody-treated groups, and normal mouse brains (closed diamonds). There were significant differences between UT and all other groups (* $p < 0.05$ ($p = 0.02$); ** $p < 0.01$ ($p = 0.007$); **** $p < 0.0001$), as well as between normal brain and other groups (#### $p < 0.0001$). Immunohistochemistry (IHC) staining for Ki67 in normal (G), untreated (UT) (H), and antibody treatments targeting plexin-B2 (PLX) (I), SLIT-3 (SLIT3) (J), and SPON-1 (SPON1) (K). (L) Positivity values for Ki67 levels in tumor regions from UT (closed circles), PLX (open squares), SLIT3 (closed triangles), and SPON1 (open inverted triangles) antibody-treated groups, and normal mouse brains (closed diamonds). There were significant differences between UT and all other groups (except between UT and SLIT3) (* $p < 0.05$ ($p = 0.03$); ** $p < 0.01$ ($p = 0.005$); **** $p < 0.0001$), as well as between normal brain and other groups (#### $p < 0.0001$). All histology slides are 20× magnifications. $n = 4$ /group. (M) Antibody treatment schematic and summarized results. ANOVA testing (one-way, multiple comparisons—Tukey’s multiple comparisons test) was used to assess the differences between means of untreated and anti-PLXNB2, anti-SLIT3- or anti-SPON1-treated GL261 glioma mice for CD44v6 or Ki67 IHC positivity levels in tumor and contralateral regions.

3.5. Bioinformatic Associations of Genes and Proteins for PLXNB2, SLIT3, or SPON1

The most recent GAMMA-predicted associations for PLXNB2, SLIT3, and SPON1 are shown in Supplementary Table S1. Note that the predictions are similar to and consistent with, but not identical to, the GAMMA predictions generated in the original 2013 paper [8] that prompted us to investigate these genes. This is because more expression data and more literature data were used in this most recent version. A summary of common and uncommon GAMMA-predicted associations for PLXNB2, SLIT3, and SPON1 is shown in Table 1. All three biomarkers are highly associated with both tumor cell proliferation and migration (both PLXNB2 and SPON1 are associated with CD44), which provides some rationale for assessing Ki67 (proliferation marker) and CD44v6 (migration marker) via IHC in the GL261 mouse model. In addition, all three biomarkers are associated with gliomas, glioblastomas, poor prognosis, and Wnt signaling. Both SLIT3 and SPON1 are highly associated with angiogenesis. Both SLIT3 and SPON1 are also highly associated with the transforming growth factor β 1 (TGF β 1), and SLIT3 seems to be also associated with NOTCH1.

Table 1. Summary of some common and uncommon GAMMA-predicted associations for PLXNB2, SLIT3, and SPON1.

Predicted Associations	PLXNB2 (Rank)	SLIT3 (Rank)	SPON1 (Rank)
Plasma membrane	X (4)		
Extracellular matrix proteins	X (65)	X (10)	
Angiogenesis		X (27)	X (14)
Cell growth	X (5)		
Cell migration	X (6)	X (22)	X (5)
Cell proliferation	X (45)	X (83)	X (33)
Cell adhesion	X (16)	X (42)	
Cell differentiation			X (68)
Glioma	X (7)	X (112)	X (13)
Glioblastoma	X (19)	X (122)	X (20)
Poor prognosis	X (24)	X (102)	X (23)
Tumor microenvironment	X (70)	X (121)	
Basement membrane		X (55)	X (28)

Table 1. *Cont.*

Predicted Associations	PLXNB2 (Rank)	SLIT3 (Rank)	SPON1 (Rank)
CD44	X (61)		X (26)
TGFB1		X (19)	X (15)
NOTCH1		X (75)	
Wnt	X (27)	X (49)	X (24)

Genetic and proteomic associations for PLXNB2, SLIT3, and SPON1 are shown in Figure 5. PLXNB2 was found to interact with several members of the semaphorin family. SPON1 was associated with several ADAMTS family members. SLIT3 interacts with several proteins in the Roundabout (ROBO) family.

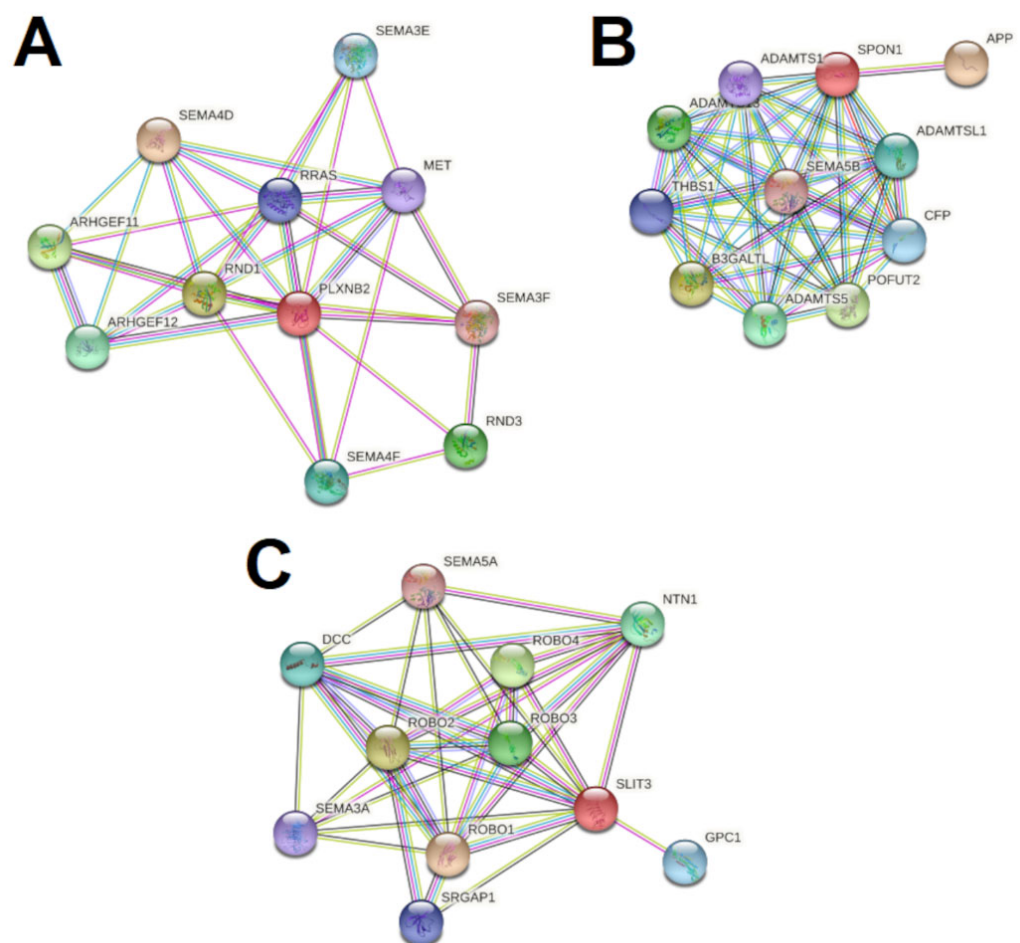


Figure 5. Protein–protein interaction neighborhoods for the biomarker candidates. (A) Plexin B2 (PLXNB2) interacts with several members of the semaphoring family, which regulate axonal growth cone guidance during development. (B) Spondin-1 (SPON1) interacts with several ADAMTS family members, enzymes involved in pathophysiological tissue remodeling during both inflammation-induced conditions as well as development. (C) SLIT3, also involved in growth guidance during development, interacts with several proteins in the Roundabout (ROBO) family.

4. Discussion

We were able to demonstrate that antibodies against PLXNB2, SLIT3, and SPON1 were all effective in significantly reducing tumor volumes (as detected by morphological MRI) and in increasing animal survival (particularly for PLXNB2 and SLIT3) when compared to untreated GL261 tumors. Antibody treatment against SPON1 was near significance

regarding animal survival, indicating that possibly a larger sample size may be required. All three of these biomarkers were also found to be highly expressed in high-grade human gliomas (as determined from IHC), as well as in the mouse GL261 orthotopic preclinical model (as measured by mt-MRI).

All three of these biomarkers (PLXNB2, SLIT3, and SPON1) are specifically associated, as previously reported, with various cancers and, PLXNB2 in particular, with gliomas. At the same time that we discovered the biomarkers discussed in this study, we also discovered that ELTD1 was also highly elevated in HGGs [22]. Over the past decade, we have also shown that antibody therapy against ELTD1 is effective in the mouse GL261 and human xenograft G55 HGG models [16,17,24]. In this study, we showed that antibody therapies against PLXNB2, SLIT3, or SPON1 were all effective in a mouse GL261 HGG model. Future studies will involve testing antibody therapies against PLXNB2, SLIT3, or SPON1 in human xenograft models.

By targeting either PLXNB2 or SPON1, it seems that this would have an effect on HGG cell migration and invasion (gene and IHC data), as well as tumor cell proliferation (IHC data); whereas targeting SLIT3 seems to mainly affect cell invasion (gene and IHC data), but is implied to also affect cell proliferation (gene data, but not supported by IHC). Future studies are required to confirm the mechanisms of action (MOAs) of the antibody therapies targeting PLXNB2, SLIT3, or SPON1 beyond what has been shown with our initial bioinformatics assessments. Preliminary bioinformatics (GAMMA)-predicted associations indicate that all three biomarkers are not only highly associated with tumor cell proliferation and migration, but also highly associated with Wnt signaling. It is important to note that blocking Wnt signaling inhibits isocitrate dehydrogenase 1 wild-type (IDH1^{WT}) GBM cell migration and proliferation [25]. Future studies should further investigate the role of Wnt signaling for these three biomarkers. Two other pathways that are associated with SLIT3 expression are TGF β 1 and NOTCH1, which both regulate tumor cell proliferation and migration, as well as angiogenesis and apoptosis [22,26]. SPON1 is also highly associated with TGF β 1. These pathways should be further investigated.

Also, we only presented preliminary data regarding the expressions of these biomarkers in human HGGs, and a larger cohort of patient samples should be assessed in future studies. The preliminary study did, however, show the translational importance of these biomarkers in human HGGs. Future studies should also take into consideration IDH1^{WT} and IDH1 mutation (R132H) characteristics, which also separate HGGs (particularly GBM [25]) and LGGs [27], respectively. It is important to note that the GL261 mouse glioma model expresses IDH1^{WT} [25], and therefore represents a validated GBM model. All three of these biomarkers were found to be highly expressed in vivo within the GL261 mouse model using a novel mt-MRI approach.

GAMMA uses literature mining to identify associations between genes and diseases such as gliomas (and synonymous terms). In reference to updated classifications, such as the new CNS5 WHO classification for adult high-grade and diffuse gliomas [1], this would only impact GAMMA-associated predictions if the data contained a new term. Importantly, predicted associations rely upon prior literature, which will not be updated when new terminology is included. Moreover, standardized schemas often contain specific phrases, which are often not used verbatim when writing, often making matching more difficult. A summary of the genes and proteins found to be associated with each of the biomarkers following GAMMA and STRING analyses is discussed in more detail below.

4.1. PLXNB2

PLXNB2 has been found to stimulate the invasive growth of malignant gliomas and may be a prognostic marker for glioma malignancy [28]. More recently, PLXNB2, which is highly expressed in glioma stem cells, was found to facilitate GBM infiltration via the modulation of cell biomechanics (e.g., lowers cellular adhesion, facilitates cytoskeletal dynamics, and forces overexpression on the actomyosin network distribution) [29].

Regarding PLXNB2 gene associations, it seems that the semaphorin (SEMA) family plays a major role, along with the Rho guanine nucleotide exchange factor (ARHGEF) family, as well as Rho GTPase Rnd1 and MET. It has been previously demonstrated that *Sema3E*-Plexin B1 signaling drives human cancer cell invasiveness and metastatic spreading in mice [30]. Another group previously suggested that Plexin-B1 could be a potential diagnostic marker for gliomas [31]. *SEMA4D* seems to be associated with Plexin-B1 in their expressions in various malignancies; however, not in breast cancer [32]. *SEMA4F* has been found to be overexpressed in a subpopulation of GBM patients that have poor survival outcomes [33]. *SEMA3G* is a potential target for antitumor migration and invasion in gliomas [34]. *ARHGEF11* promotes the proliferation and epithelial-mesenchymal transition of hepatocellular carcinoma through the activation of the β -catenin pathway [35]. *ARHGEF12* is widely associated with leukemias and is also known as the Leukemia-Associated Rho Guanine Nucleotide Exchange Factor [36]. *RND3* has been found to promote Snail 1 protein degradation, which results in the inhibition of glioblastoma cell migration and invasion [37]. *RND1* is up-regulated in esophageal squamous cell carcinoma and promotes the growth and migration of cancer cells [38]. Lastly, MET and its ligand hepatocyte growth factor (HGF) play a critical role in the proliferation, survival, migration, invasion, angiogenesis, and stem cell characteristics and in the therapeutic resistance and recurrence of glioblastomas [39].

4.2. *SLIT3*

SLIT3 was found previously to be hypermethylated in glioma and colorectal cancer cell lines [40]. The methylation of *SLIT3* was found both in early gastric cancers and in advanced gastric cancers [41]. *SLIT3* was widely expressed in human hepatocellular carcinomas [42], and, more recently, in non-small-cell lung cancer [43]. The Slit/Robo signaling pathway is reportedly involved in breast cancer development and metastasis [44].

From gene associations for *SLIT3*, the Slit/Robo signaling pathway plays an important role in glioma cell migration [45], as well as *SEMA3A*, *DCC* (deleted in colorectal cancer), *netrin-1* (*NTN1*), *SRGAP1* (*SLIT-ROBO* Rho GTPase-activating protein 1), and *GPC1* (*glypican-1*). *Sema5A* has been found to regulate human glioma cell motility and morphology [46], and *Semaphorin 3A* (*SEMA3A*) is involved in mediating brain tumor cell proliferation and invasion in *EGFR* mutant gliomas [47]. It has been previously reported that the loss of *DCC* expression may be closely related to changes in cell kinetics and tumor phenotype in astrocytomas, independent of p53 abnormalities [48]. The *netrin-1* (*NTN1*)-induced activation of Notch signaling mediates glioblastoma cell invasion [49]. *srGAP1* is known to be involved in GBM cell invasion [50]. Lastly, high expression of *GPC1* predicts dissemination and poor prognosis in glioblastomas [51].

4.3. *SPON1*

SPON1 was previously found to be overexpressed in ovarian/peritoneal carcinomas [52], gastric cancer [53], and osteosarcoma [12]. *SPON1* has also been reported to promote metastasis in human osteosarcoma [12].

In reference to *SPON1* gene associations, this gene interacts with several genes from *ADAMTS* (zinc-dependent endopeptidases) family members, as well as *SEMA5B*, *POFUT2* (associated with fucose metabolism), and *THBS1* (*thrombospondin-1*). The extracellular protease *ADAMTS1* plays a role in glioma through its action on *IGFBP2* (*insulin-like growth factor-binding protein 2*) [54]. Matrix-degrading proteases *ADAMTS4* and *ADAMTS5* (*disintegrins* and *metalloproteinases* with *thrombospondin* motifs 4 and 5) are highly expressed in human glioblastomas [55]. It has been speculated that *APP* could affect the migration and invasion of human breast cancer cells by mediating the activation of the *MAPK* signaling pathway, thereby promoting the *EMT* process [56]. *SEMA5B* is thought to be an effective diagnostic marker and a possible therapeutic target for clear cell renal carcinoma [57]. Histology-based expression profiling yielded the novel prognostic marker, *POFUT2*, associated with fucose metabolism, for human glioblastoma [58]. *TGF β 1* induces

THBS1 expression via Smad3 which contributes to the invasive behavior during GBM expansion [59].

5. Conclusions

In this study, we validated the therapeutic potential of targeting PLXNB2, SLIT3, or SPON1 by showing that using antibodies to block these biomarkers (PLXNB2, SLIT3, SPON1) results in significant increases in mouse survival in treated GL261 tumor-bearing mice (particularly for antibody treatments against PLXNB2 and SLIT3) compared to untreated tumor-bearing mice. There were also significant decreases in tumor volumes for antibody-treated mice against all three biomarkers compared to untreated mice. In addition, mt-MRI indicated that all three of these biomarkers were substantially elevated in the tumor regions of untreated GL261-tumor-bearing mice. A preliminary bioinformatics assessment indicated that these three biomarkers are highly associated with tumor cell proliferation and migration and may have a common Wnt signaling association. More mechanistic studies are required to confirm the MOAs for each biomarker in high-grade gliomas. These preliminary results indicate that targeting these three biomarkers could potentially add to the therapeutic arsenal against high-grade gliomas and that antibodies against them may be considered for future clinical translation.

Supplementary Materials: The following supporting information can be downloaded at: <https://www.mdpi.com/article/10.3390/neuroglia4010006/s1>, Table S1: Complete GAMMA data for gene associations for Plexin-B2, SLIT-3 and Spondin-1.

Author Contributions: Conceptualization, R.A.T. and J.D.W.; methodology, R.A.T., J.D.W., R.L.J., N.S. and M.L.; validation, N.S., R.L.J. and M.L.; formal analysis, R.A.T., J.D.W., R.L.J., N.S. and D.S.; investigation, R.A.T. and J.D.W.; resources, R.A.T. and J.D.W.; data curation, J.D.W., D.S., M.L. and J.D.W.; writing—original draft preparation, R.A.T.; writing—review and editing, M.A., J.D.W., J.B., R.L.J., N.S. and D.S.; visualization, R.A.T., M.A., R.L.J. and J.D.W.; supervision, R.A.T.; project administration, R.A.T.; funding acquisition, R.A.T. and J.D.W. All authors have read and agreed to the published version of the manuscript.

Funding: This research was funded by the Oklahoma Medical Research Foundation (no specific grant no.) to RAT and The National Institutes of Health (S10OD023508) to RAT, (P20GM103636) to JDW, and (U54GM104938) to JDW. Whole-slide scanning and image analysis were kindly provided by the Peggy and Charles Stephenson Cancer Center at the University of Oklahoma Health Sciences Center, through an Institutional Development Award (IDeA) from the National Institute of General Medical Sciences (P20GM103639) and a Cancer Center Supporting Grant Award from the National Cancer Institute (P30CA225520).

Institutional Review Board Statement: The study was conducted in accordance with the Declaration of Helsinki and approved by the Institutional Review Board (or Ethics Committee) of the University of Utah Health Sciences Center (protocol IRB 10924, approved 13 December 2002). The animal study protocol was approved by the Institutional Review Board (or Ethics Committee) of the Oklahoma Medical Research Foundation (protocol code 14-03, approved 24 February 2014).

Informed Consent Statement: Patient consent was waived as only deidentified tissue was used for our study.

Data Availability Statement: Research data are available upon request.

Acknowledgments: We would like to thank the following summer research students for their assistance: Landon Rodriguez, Mary Girton, and Rick Pody. We would like to thank Constantin Georgescu for providing statistical support.

Conflicts of Interest: The authors declare no conflict of interest. The funders had no role in the design of the study; in the collection, analyses, or interpretation of data; in the writing of the manuscript; or in the decision to publish the results.

References

1. Louis, D.; Perry, A.; Wesseling, P.; Brat, D.; Cree, I.; Figarella-Branger, D.; Hawkins, C.; Ng, H.K.; Pfister, S.; Reifenberger, G.; et al. The 2021 WHO Classification of Tumors of the Central Nervous System: A summary. *Neuro-Oncology* **2021**, *23*, 1231–1251. [[CrossRef](#)]
2. Basile, J.R.; Barac, A.; Zhu, T.; Guan, K.L.; Gutkind, J.S. Class IV semaphorins promote angiogenesis by stimulating Rho-initiated pathways through plexin-B. *Cancer Res.* **2004**, *64*, 5212–5224. [[CrossRef](#)] [[PubMed](#)]
3. Yang, K.; Wu, Z.; Zhang, H.; Zhang, N.; Wu, W.; Wang, Z.; Dai, Z.; Zhang, X.; Zhang, L.; Peng, Y.; et al. Glioma targeted therapy: Insight into future of molecular approaches. *Mol. Cancer* **2022**, *21*, 39. [[CrossRef](#)] [[PubMed](#)]
4. Nicholson, J.G.; Fine, H.A. Diffuse Glioma Heterogeneity and Its Therapeutic Implications. *Cancer Discov.* **2021**, *11*, 575–590. [[CrossRef](#)]
5. Singh, G.; Manjila, S.; Sakla, N.; True, A.; Wardeh, A.H.; Beig, N.; Vaysberg, A.; Matthews, J.; Prasanna, P.; Spektor, V. Radiomics and radiogenomics in gliomas: A contemporary update. *Br. J. Cancer* **2021**, *125*, 641–657. [[CrossRef](#)] [[PubMed](#)]
6. Jang, K.; Russo, C.; Di Ieva, A. Radiomics in gliomas: Clinical implications of computational modeling and fractal-based analysis. *Neuroradiology* **2020**, *62*, 771–790. [[CrossRef](#)]
7. Li, D.; Patel, C.B.; Xu, G.; Iagaru, A.; Zhu, Z.; Zhang, L.; Cheng, Z. Visualization of Diagnostic and Therapeutic Targets in Glioma with Molecular Imaging. *Front. Immunol.* **2020**, *11*, 592389. [[CrossRef](#)]
8. Towner, R.A.; Jensen, R.L.; Vaillant, B.; Colman, H.; Saunders, D.; Giles, C.B.; Wren, J. Experimental validation of 5 in-silico predicted glioma biomarkers. *Neuro-Oncology* **2013**, *15*, 1625–1634. [[CrossRef](#)]
9. Holl, E.K.; Roney, K.E.; Allen, I.C.; Steinbach, E.; Arthur, J.C.; Buntzman, A.; Plevy, S.; Frelinger, J.; Ting, J.P. Plexin-B2 and Plexin-D1 in dendritic cells: Expression and IL-12/IL-23p40 production. *PLoS ONE* **2012**, *7*, e43333. [[CrossRef](#)]
10. Roney, K.E.; O'Connor, B.P.; Wen, H.; Holl, E.K.; Guthrie, E.H.; Davis, B.K.; Jones, S.W.; Jha, S.; Sharek, L.; García-Mata, R.; et al. Plexin-B2 Negatively Regulates Macrophage Motility, Rac, and Cdc42 Activation. *PLoS ONE* **2011**, *6*, e24795. [[CrossRef](#)]
11. Jiang, Z.; Liang, G.; Xiao, Y.; Qin, T.; Chen, X.; Wu, E.; Ma, Q.; Wang, Z. Targeting the SLIT/ROBO pathway in tumor progression: Molecular mechanisms and therapeutic perspectives. *Ther. Adv. Med. Oncol.* **2019**, *11*, 1758835919855238. [[CrossRef](#)] [[PubMed](#)]
12. Chang, H.; Dong, T.; Ma, X.; Zhang, T.; Chen, Z.; Yang, Z.; Zhang, Y. Spondin 1 promotes metastatic progression through Fak and Src dependent pathway in human osteosarcoma. *Biochem. Biophys. Res. Commun.* **2015**, *464*, 45–50. [[CrossRef](#)] [[PubMed](#)]
13. Zhang, L.; Song, Y.; Ling, Z.; Li, Y.; Ren, X.; Yang, J.; Wang, Z.; Xia, J.; Zhang, W.; Cheng, B. R-spondin 2-LGR4 system regulates growth, migration and invasion, epithelial-mesenchymal transition and stem-like properties of tongue squamous cell carcinoma via Wnt/ β -catenin signaling. *EBioMedicine* **2019**, *44*, 275–288. [[CrossRef](#)]
14. Wick, W.; Platten, M.; Weller, M. Glioma cell invasion: Regulation of metalloproteinase activity by TGF-beta. *J. Neurooncol.* **2001**, *53*, 177–185. [[CrossRef](#)] [[PubMed](#)]
15. Furnari, F.; Cavenee, W.K. Targeting EGFR for Treatment of Glioblastoma: Molecular Basis to Overcome Resistance. *Curr. Cancer Drug Targets* **2012**, *12*, 197–209. [[CrossRef](#)]
16. Ziegler, J.; Pody, R.; de Souza, P.C.; Evans, B.; Saunders, D.; Smith, N.; Mallory, S.; Njoku, C.; Dong, Y.; Chen, H.; et al. ELTD1, an effective anti-angiogenic target for gliomas: Preclinical assessment in mouse GL261 and human G55 xenograft glioma models. *Neuro-Oncology* **2016**, *19*, 175–185. [[CrossRef](#)]
17. Zalles, M.; Smith, N.; Ziegler, J.; Saunders, D.; Remerowski, S.; Thomas, L.; Gulej, R.; Mamedova, N.; Lerner, M.; Fung, K.; et al. Optimized monoclonal antibody treatment against ELTD1 for GBM in a G55 xenograft mouse model. *J. Cell Mol. Med.* **2019**, *24*, 1738–1749. [[CrossRef](#)]
18. Jensen, R.L. Brain tumor hypoxia: Tumorigenesis, angiogenesis, imaging, pseudoprogression, and as a therapeutic target. *J. Neuro-Oncol.* **2009**, *92*, 317–335. [[CrossRef](#)]
19. Dozmorov, M.G.; Giles, C.B.; Wren, J.D. Predicting gene ontology from a global meta-analysis of 1-color microarray experiments. *BMC Bioinform.* **2011**, *12*, S14. [[CrossRef](#)]
20. Fields, E.; Wren, J.D.; Georgescu, C.; Daum, J.R.; Gorbosky, G.J. Predictive bioinformatics identifies novel regulators of proliferation in a cancer stem cell model. *Stem Cell Res.* **2017**, *26*, 1–7. [[CrossRef](#)]
21. Tipton, A.R.; Wren, J.D.; Daum, J.R.; Siefert, J.C.; Gorbosky, G.J. GTSE1 regulates spindle microtubule dynamics to control Aurora B kinase and Kif4A chromokinesin on chromosome arms. *J. Cell Biol.* **2017**, *216*, 3117–3132. [[CrossRef](#)] [[PubMed](#)]
22. Towner, R.A.; Jensen, R.L.; Colman, H.; Vaillant, B.; Smith, N.; Casteel, R.; Saunders, D.; Gillespie, D.L.; Silasi-Mansat, R.; Lupu, F.; et al. ELTD1, a Potential New Biomarker for Gliomas. *Neurosurgery* **2013**, *72*, 77–91. [[CrossRef](#)]
23. Szklarczyk, D.; Gable, A.L.; Nastou, K.C.; Lyon, D.; Kirsch, R.; Pyysalo, S.; Doncheva, N.T.; Legeay, M.; Fang, T.; Bork, P.; et al. The STRING database in 2021: Customizable protein-protein networks, and functional characterization of user-uploaded gene/measurement sets. *Nucleic Acids Res.* **2021**, *49*, D60–D612. [[CrossRef](#)]
24. Zalles, M.; Smith, N.; Saunders, D.; Guzman, M.; Lerner, M.; Fung, K.-M.; Babu, A.; Battiste, J.; Chung, J.; Hwang, K.; et al. ELTD1 as a multi-focal target for malignant gliomas: Preclinical studies. *Neuro-Oncol. Adv.* **2021**, *3*, vdab132. [[CrossRef](#)] [[PubMed](#)]
25. Fan, D.; Yue, Q.; Chen, J.; Wang, C.; Yu, R.; Jin, Z.; Yin, S.; Wang, Q.; Chen, L.; Liao, X.; et al. Reprogramming the immunosuppressive microenvironment of IDH1 wild-type glioblastoma by blocking Wnt signaling between microglia and cancer cells. *Oncoimmunology* **2021**, *10*, 1932061. [[CrossRef](#)] [[PubMed](#)]

26. Towner, R.A.; Smith, N.; Saunders, D.; Brown, C.A.; Cai, X.; Ziegler, J.; Mallory, S.; Dozmorov, M.G.; Coutinho De Souza, P.; Wiley, G.; et al. OKN-007 Increases temozolomide (TMZ) Sensitivity and Sup-presses TMZ-Resistant Glioblastoma (GBM) Tumor Growth. *Transl. Oncol.* **2019**, *12*, 320–335. [[CrossRef](#)] [[PubMed](#)]
27. Pellegatta, S.; Valletta, L.; Corbetta, C.; Patanè, M.; Zucca, I.; Riccardi Sirtori, F.; Bruzzone, M.G.; Fogliatto, G.; Isacchi, A.; Pollo, B.; et al. Effective immuno-targeting of the IDH1 mutation R132H in a murine model of intracranial glioma. *Acta Neuropathol. Commun.* **2015**, *3*, 4. [[CrossRef](#)]
28. Le, A.P.; Huang, Y.; Pingle, S.C.; Kesari, S.; Wang, H.; Yong, R.L.; Zou, H.; Friedel, R.H. Plexin-B2 promotes invasive growth of malignant glioma. *Oncotarget* **2015**, *6*, 7293–7304. [[CrossRef](#)] [[PubMed](#)]
29. Huang, Y.; Tejero, R.; Lee, V.K.; Brusco, C.; Hannah, T.; Bertucci, T.B.; Alves, C.J.; Katsyv, I.; Kluge, M.; Foty, R.; et al. Plexin-B2 facilitates glioblastoma infiltration by modulating cell biomechanics. *Commun. Biol.* **2021**, *4*, 145. [[CrossRef](#)]
30. Casazza, A.; Finisguerra, V.; Capparuccia, L.; Camperi, A.; Swiercz, J.M.; Rizzolio, S.; Rolny, C.; Christensen, C.; Bertotti, A.; Sarotto, I.; et al. Sema3E–Plexin D1 signaling drives human cancer cell invasiveness and metastatic spreading in mice. *J. Clin. Investig.* **2010**, *120*, 2684–2698. [[CrossRef](#)]
31. Zhang, Y.; Li, Q.; Zhuang, R.; Gao, Z.; Liu, J.; Li, J.; Yang, A.; Cheng, G.; Jin, B. Plexin-B1: A potential diagnostic biomarker for glioma and a future target for glioma immunotherapy. *J. Neuroimmunol.* **2012**, *252*, 113–117. [[CrossRef](#)] [[PubMed](#)]
32. Yang, Y.; Wang, J.; Li, H.; Liu, L.; Yao, M.; Xiao, T. Association between prognosis and SEMA4D/Plexin-B1 expression in various malignancies: A meta-analysis. *Medicine* **2019**, *98*, e13298. [[CrossRef](#)]
33. Shergalis, A.; Bankhead, A., 3rd; Luesakul, U.; Muangsins, N.; Neamati, N. Current Challenges and Opportunities in Treating Glioblastoma. *Pharmacol. Rev.* **2018**, *70*, 412–445. [[CrossRef](#)]
34. Yu, R.; Zhou, X.; Ma, L.; Li, J.; Gu, J.; Shi, Q. Effects of SEMA3G on migration and invasion of glioma cells. *Oncol. Rep.* **2012**, *28*, 269–275. [[CrossRef](#)]
35. Du, J.; Zhu, Z.; Xu, L.; Chen, X.; Li, X.; Lan, T.; Li, W.; Yuan, K.; Zeng, Y. ARHGEF11 promotes proliferation and epitheli-al-mesenchymal transition of hepatocellular carcinoma through activation of β -catenin pathway. *Aging* **2020**, *12*, 20235–20253. [[CrossRef](#)]
36. Beveridge, R.D.; Staples, C.J.; Patil, A.A.; Myers, K.N.; Maslen, S.; Skehel, J.M.; Boulton, S.J.; Collis, S.J. The leukemia-associated Rho guanine nucleotide exchange factor LARG is required for efficient replication stress signaling. *Cell Cycle* **2014**, *13*, 3450–3459. [[CrossRef](#)] [[PubMed](#)]
37. Liu, B.; Dong, H.; Lin, X.; Yang, X.; Yue, X.; Yang, J.; Li, Y.; Wu, L.; Zhu, X.; Zhang, S.; et al. RND3 promotes Snail 1 protein degradation and inhibits glioblastoma cell migration and invasion. *Oncotarget* **2016**, *7*, 82411–82423. [[CrossRef](#)] [[PubMed](#)]
38. Xiang, G.; Yi, Y.; Weiwei, H.; Weiming, W. RND1 is up-regulated in esophageal squamous cell carcinoma and promotes the growth and migration of cancer cells. *Tumor Biol.* **2015**, *37*, 773–779. [[CrossRef](#)] [[PubMed](#)]
39. Cheng, F.; Guo, D. MET in glioma: Signaling pathways and targeted therapies. *J. Exp. Clin. Cancer Res.* **2019**, *38*, 270. [[CrossRef](#)]
40. Dickinson, R.E.; Dallol, A.; Bieche, I.; Krex, D.; Morton, D.; Maher, E.R.; Latif, F. Epigenetic inactivation of SLIT3 and SLIT1 genes in human cancers. *Br. J. Cancer* **2004**, *91*, 2071–2078. [[CrossRef](#)]
41. Kim, M.; Kim, J.H.; Baek, S.J.; Kim, S.Y.; Kim, Y.S. Specific expression and methylation of SLIT1, SLIT2, SLIT3, and miR-218 in gastric cancer subtypes. *Int. J. Oncol.* **2016**, *48*, 2497–2507. [[CrossRef](#)]
42. Lin, Z.Y.; Chuang, W.L. Genes responsible for the characteristics of primary cultured invasive phenotype hepatocellular carcinoma cells. *Biomed. Pharm.* **2012**, *66*, 454–458. [[CrossRef](#)]
43. Jin, X.; Guan, Y.; Zhang, Z.; Wang, H. Microarray data analysis on gene and miRNA expression to identify biomarkers in non-small cell lung cancer. *BMC Cancer* **2020**, *20*, 329. [[CrossRef](#)]
44. Gu, F.; Ma, Y.; Zhang, J.; Qin, F.; Fu, L. Function of Slit/Robo signaling in breast cancer. *Front. Med.* **2015**, *9*, 431–436. [[CrossRef](#)] [[PubMed](#)]
45. Han, P.-P.; Zhang, G.-Q.; Li, L.; Yue, L. Downregulation of USP33 inhibits Slit/Robo signaling pathway and is associated with poor patient survival of glioma. *J. Neurosurg. Sci.* **2023**, *67*, 113–120. [[CrossRef](#)]
46. Li, X.; Law, J.W.S.; Lee, A.Y.W. Semaphorin 5A and plexin-B3 regulate human glioma cell motility and morphology through Rac1 and the actin cytoskeleton. *Oncogene* **2011**, *31*, 595–610. [[CrossRef](#)] [[PubMed](#)]
47. Higgins, D.M.O.; Caliva, M.; Schroeder, M.; Carlson, B.; Upadhyayula, P.S.; Milligan, B.D.; Cheshier, S.H.; Weissman, I.L.; Sarkaria, J.N.; Meyer, F.B.; et al. Semaphorin 3A mediated brain tumor stem cell proliferation and invasion in EGFRviii mutant gliomas. *BMC Cancer* **2020**, *20*, 1213. [[CrossRef](#)] [[PubMed](#)]
48. Hara, A.; Saegusa, M.; Mikami, T.; Okayasu, I. Loss of DCC expression in astrocytomas: Relation to p53 abnormalities, cell kinetics, and survival. *J. Clin. Pathol.* **2001**, *54*, 860–865. [[CrossRef](#)] [[PubMed](#)]
49. Ylivinkka, L.; Hu, Y.; Chen, P.; Rantanen, V.; Hautaniemi, S.; Nyman, T.; Keski-Oja, J.; Hyytiäinen, M. Netrin-1 induced activation of Notch signaling mediates glioblastoma cell invasion. *J. Cell Sci.* **2013**, *126*, 2459–2469. [[CrossRef](#)] [[PubMed](#)]
50. Koo, S.; Martin, G.; Toussaint, L.G. MicroRNA-145 Promotes the Phenotype of Human Glioblastoma Cells Selected for Invasion. *Anticancer Res.* **2015**, *35*, 3209–3215.
51. Saito, T.; Sugiyama, K.; Hama, S.; Yamasaki, F.; Takayasu, T.; Nosaka, R.; Onishi, S.; Muragaki, Y.; Kawamata, T.; Kurisu, K. High Expression of Glypican-1 Predicts Dissemination and Poor Prognosis in Glioblastomas. *World Neurosurg.* **2017**, *105*, 282–288. [[CrossRef](#)] [[PubMed](#)]

52. Davidson, B.; Stavnes, H.T.; Holth, A.; Chen, X.; Yang, Y.; Shih, I.E.M.; Wang, T.L. Gene expression signatures differentiate ovari-an/peritoneal serous carcinoma from breast carcinoma in effusions. *J. Cell Mol. Med.* **2011**, *15*, 535–544. [[CrossRef](#)] [[PubMed](#)]
53. Ding, Y.; Chen, Y.; Wu, M.; Li, L.; Huang, Y.; Wang, H.; Wang, H.; Yu, X.; Xu, N.; Teng, L. Identification of genes associated with gastric cancer survival and construction of a nomogram to improve risk stratification for patients with gastric cancer. *Oncol. Lett.* **2020**, *20*, 215–225. [[CrossRef](#)]
54. Serrano-Garrido, O.; Peris-Torres, C.; Redondo-García, S.; Asenjo, H.G.; Plaza-Calonge, M.D.C.; Fernandez-Luna, J.L.; Rodríguez-Manzanegue, J.C. ADAMTS1 Supports Endothelial Plasticity of Glioblastoma Cells with Relevance for Glioma Progression. *Biomolecules* **2020**, *11*, 44. [[CrossRef](#)]
55. Held-Feindt, J.; Paredes, E.B.; Blömer, U.; Seidenbecher, C.; Stark, A.M.; Mehdorn, H.M.; Mentlein, R. Matrix-degrading proteases ADAMTS4 and ADAMTS5 (disintegrins and metalloproteinases with thrombospondin motifs 4 and 5) are expressed in human glioblastomas. *Int. J. Cancer* **2005**, *118*, 55–61. [[CrossRef](#)]
56. Wu, X.; Chen, S.; Lu, C. Amyloid precursor protein promotes the migration and invasion of breast cancer cells by regulating the MAPK signaling pathway. *Int. J. Mol. Med.* **2019**, *45*, 162–174. [[CrossRef](#)] [[PubMed](#)]
57. Hirota, E.; Yan, L.; Tsunoda, T.; Ashida, S.; Fujime, M.; Shuin, T.; Miki, T.; Nakamura, Y.; Katagiri, T. Genome-wide gene expression profiles of clear cell renal cell carcinoma: Identification of molecular targets for treatment of renal cell carcinoma. *Int. J. Oncol.* **2006**, *29*, 799–827. [[CrossRef](#)] [[PubMed](#)]
58. Dong, S.; Nutt, C.L.; Betensky, R.A.; Stemmer-Rachamimov, A.O.; Denko, N.C.; Ligon, K.L.; Rowitch, D.; Louis, D.N. Histology-Based Expression Profiling Yields Novel Prognostic Markers in Human Glioblastoma. *J. Neuropathol. Exp. Neurol.* **2005**, *64*, 948–955. [[CrossRef](#)]
59. Daubon, T.; Léon, C.; Clarke, K.; Andrique, L.; Salabert, L.; Darbo, E.; Pineau, R.; Guérit, S.; Maitre, M.; Dedieu, S.; et al. Deciphering the complex role of thrombospondin-1 in glioblastoma development. *Nat. Commun.* **2019**, *10*, 1146. [[CrossRef](#)]

Disclaimer/Publisher’s Note: The statements, opinions and data contained in all publications are solely those of the individual author(s) and contributor(s) and not of MDPI and/or the editor(s). MDPI and/or the editor(s) disclaim responsibility for any injury to people or property resulting from any ideas, methods, instructions or products referred to in the content.